Environmental mercury and arsenic sources in fossil hydrothermal systems, Northland, New Zealand

D. Craw · D. Chappell · A. Reay

Abstract Northland, New Zealand has been affected by natural hot water spring systems depositing elevated concentrations of mercury and arsenic over the past 5 million years. Due to the different erosion levels of these hot water systems, four principal types of mercury and arsenic occurrences are found: active hot springs; layered surface deposits (sinters) deposited by hot springs; highly fractured rock zones formed immediately beneath hot springs; and chemically altered and mineralized rock from the deeper roots of hot spring systems. Mercury occurs principally as cinnabar and as a minor impurity (<1 wt%) in phosphate minerals and iron sulfides, particularly marcasite. Mercury is irregularly distributed through limonitic cements formed during oxidation. Arsenic occurs as a minor impurity (<1 wt%) in phosphate minerals and iron sulfides, particularly marcasite. Arsenic is also variably dispersed through limonite, but not necessarily with mercury. Decomposition of marcasite constitutes the most significant source of mercury and arsenic pollution from the studied sites. Release of mercury and arsenic into the environment from marcasite, phosphates and limonite is enhanced by acidification of the sites (down to pH of 2), caused by oxidation of iron sulfides. Mercury and arsenic concentrations of up to 100 parts per billion should be expected in waters near the deposits; these concentrations are in excess of recommended drinking water levels.

Key words Marcasite · Cinnabar · Phosphates · Hot springs

Received: 9 April 1999 · Accepted: 2 August 1999

D. Craw (✉) · D. Chappell · A. Reay
Geology Department, University of Otago, P.O. Box 56, Dunedin, New Zealand
e-mail: dave.craw.@stonebow.otago.ac.nz

Introduction

Hot spring systems are notorious for their discharges of heavy metals into the environment (Axtmann 1975; Weissberg and others 1979; Ferrara and others 1991). Most hot spring waters contain at least some dissolved metals at their discharge points, and these metals are readily transferred to soil and stream systems downstream either in solution or as precipitates (Varekamp and Buseck 1983). The precipitates can be further mobilized by erosion, contributing metallic minerals to the stream sediments. Within the stream systems, dissolved and precipitated metals become periodically bioavailable depending on the solubility of the metals in local biogeochemical environments. This, in turn, can lead to toxic levels of metals in the environment in the short or long term (Axtmann 1975; Baldi 1988).

Mercury and arsenic are two heavy metals which, because they are relatively soluble metals in hot or warm hydrothermal fluids right up to the surface (White 1981) and are toxic at relatively low (ppb) levels (Turner 1993; Loebenstein 1993), commonly cause environmental problems downstream of hot spring systems (Axtmann 1975; Baldi 1988). In addition to the immediate environmental effects of hot spring discharges, hot spring systems leave metal-contaminated zones in the host rock within the immediate vicinity of the discharge point. These anomalous metal zones are important features used by mineral exploration geochemists when searching for potential precious metal deposits which can form at deeper levels in metalliferous hot spring systems (White 1981). However, these anomalous metal zones also constitute point sources for further toxic metal discharges as the rock is eroded, long after the hot spring systems have died.

The Northland area of New Zealand provides excellent examples of mercury- and arsenic-bearing hot spring systems exposed at several erosional levels, from active systems to the feeder zones originally tens of metres below the surface. Hence, the architecture of the spring systems can be observed in outcrop, and the nature of potential metallic pollution can be examined. Discharge of these metals can be accelerated by human activity such as mining or quarrying, as larger volumes of metallic minerals are exposed to oxidation and decomposition at the surface. The amounts of metals released depends on the decomposition rate of the metallic minerals present in the rocks.

This study describes the distribution of mercury and arsenic within fossil hot spring systems from a mineralogical perspective. The study then investigates the nature and rates of decomposition of the arsenic- and mercury-bearing minerals at various levels in the fossil systems. The study focuses on the Puhipuhi area of Northland where the fossil systems are best exposed. This area contains partially eroded fossil hot spring systems which were highly enriched in mercury and, to a lesser extent, in arsenic. The actual concentrations of metals in waters downstream of the studied sites depends on rainfall and sediment attenuation mechanisms. These aspects are beyond the scope of the present study but are part of ongoing work in the area.

Geological setting

Regional geology

The Northland area is underlain by a low-grade metamorphic basement of Mesozoic (ca. 200–250 Ma) greywackes and argillites with minor siliceous horizons (cherts) and mafic volcanic rocks. The basement was faulted extensively on a northerly strike in the late Cenozoic (ca. 5 Ma; Fig. 1). These faults controlled deposition of Pliocene lake and fluvial sediments in structural depressions at Ngawha and Puhipuhi (Fig. 1). Active mercury-bearing hot springs at Ngawha penetrated through the lake sediments and discharged into streams, leaving deposits of cinnabar and mobilizing mercury liquid and vapour (Henderson 1944). Eruption of terrestrial volcanic rocks was also controlled by the same northerly striking faults (White 1986; Grieve and others 1997) and lava flows were channelled by structurally-controlled topography. The volcanic rocks are predominantly basalts of Miocene to Pliocene age (5-2 Ma; Smith and others 1993). The Mesozoic basement at Puhipuhi is largely overlain by up to 40 m of basaltic lavas (Fig. 2) deposited in valleys associated with the graben. Subsequent uplift and erosion have left these valley deposits as resistant remnants, forming topographic high ground.

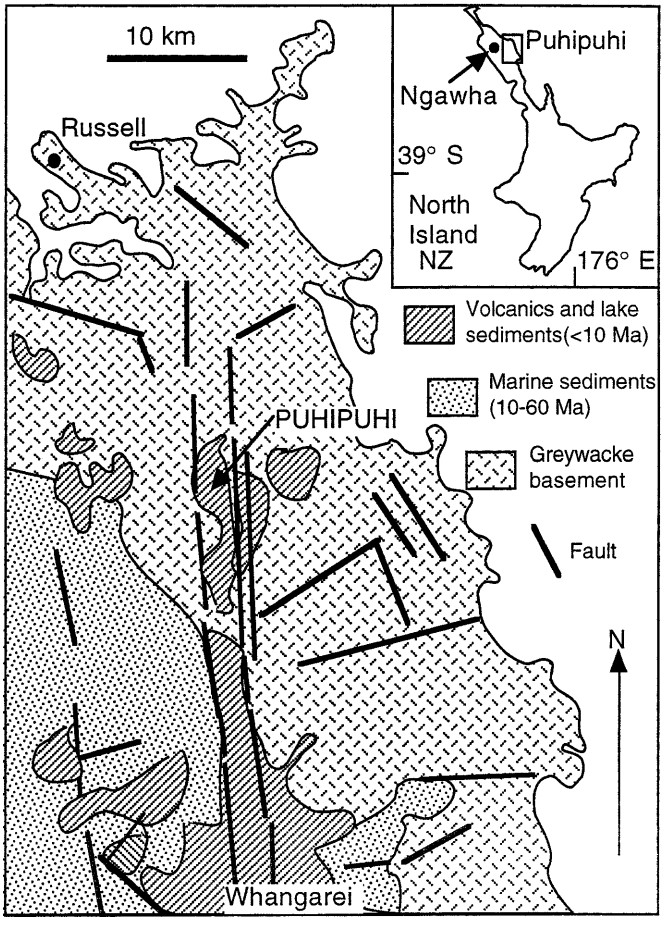

Fig. 1
Geological map of the Whangarei-Bay of Islands (Russell) region (after Kear and Hay 1961; Grieve and others 1997) showing the Puhipuhi area (see Fig. 2) in relation to regional structures. The *inset* shows the location of this region in the North Island of New Zealand

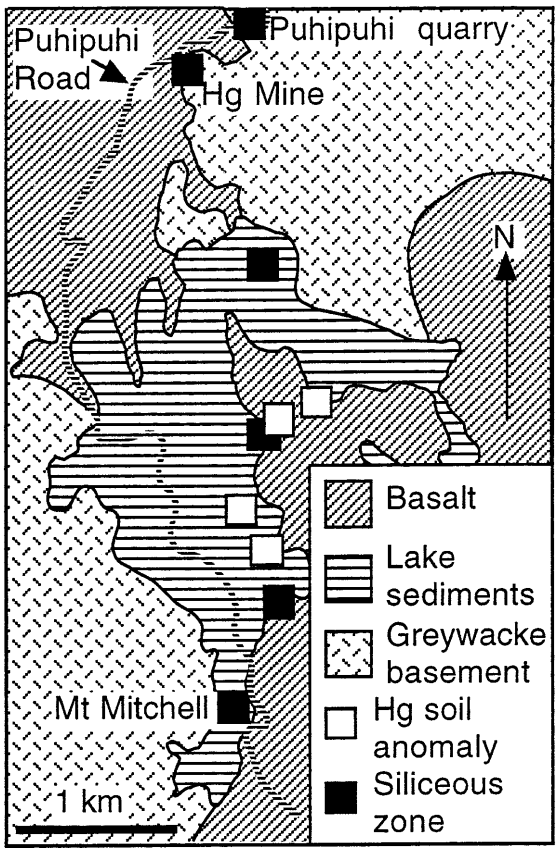

Fig. 2
Geological map of the Puhipuhi area (after Henderson 1944; Grieve and others 1997) showing the principal sites which have been hydrothermally altered with metal addition. The three sites discussed in this report are indicated

Puhipuhi mineralized localities

The Puhipuhi area has been extensively affected by hydrothermal activity locally (Fig. 2). Hydrothermal activity was controlled by the north-striking faults and associated

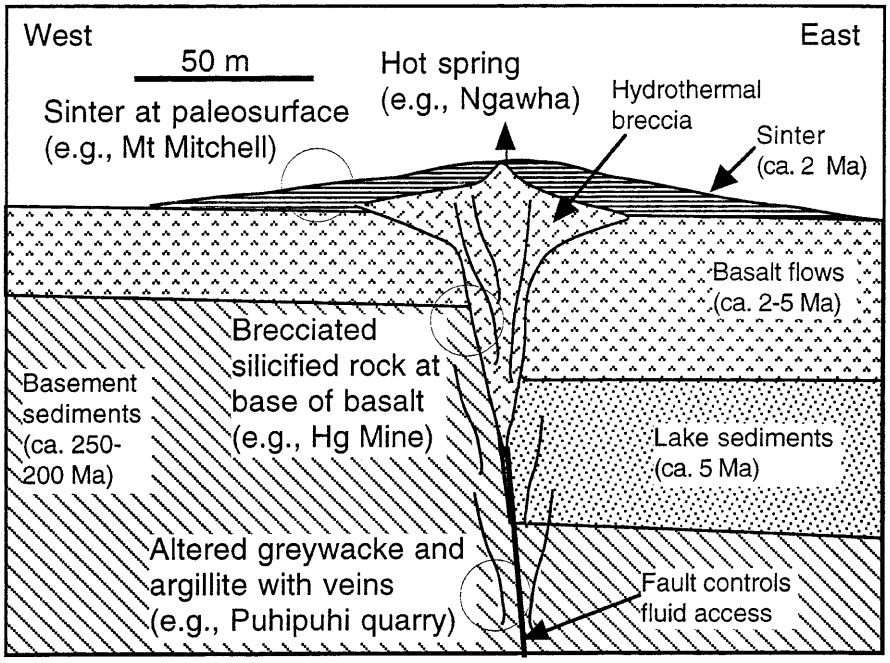

Fig. 3
Conceptual sketch cross section (after White 1986; Grieve and others 1997; not strictly to scale) through a Northland hydrothermal system, showing the different levels of the system examined in this study (*ringed*)

fractures in the basement (White 1986; Grieve and others 1997). Rocks adjacent to these structures have been variably silicified and/or altered to clay mineral assemblages, with localized metallic sulfide mineral concentrations. Some alteration was accompanied by hydrothermal brecciation (White 1986; Grieve and others 1997). Alteration of all rock types has occurred, but alteration and hydrothermal mineralization are most pronounced in the sediments and volcanics as well as at the contact between these and the underlying basement (Henderson 1944; White 1986; Grieve and others 1997). The hydrothermal activity is thought to be Plio-Pleistocene in age and to have occurred essentially at the paleosurface (White 1986; Grieve and others 1997). The general structure of these hydrothermal systems is depicted schematically in Fig. 3 (White 1986; Grieve and others 1997). These deposits have been extensively explored for gold mineralization over the past 30 years and were locally mined for mercury up to World War II. Minor excavations for road metal have also occurred.

Hydrothermal mineralization resulted in deposition of cinnabar (HgS), stibnite (Sb_2S_3), and iron sulfides, with minor gold and silver, at numerous localities in the area (Fig. 2). To give a broad overview of the range of mineralogy and mercury occurrences this study examines material from three localities with distinctly different formation styles (Mt. Mitchell, a surface deposit; Hg Mine, a near-surface breccia; and Puhipuhi quarry, a basement vein system; Figs. 2, 3). The relative positions of these three sites in a composite hydrothermal system are depicted in Fig. 3.

Description of studied localities

The hydrothermal processes resulted in localized siliceous sinter deposits at the paleosurface (Fig. 2). The most extensive of these is at Mt. Mitchell (Fig. 2) where sinter up

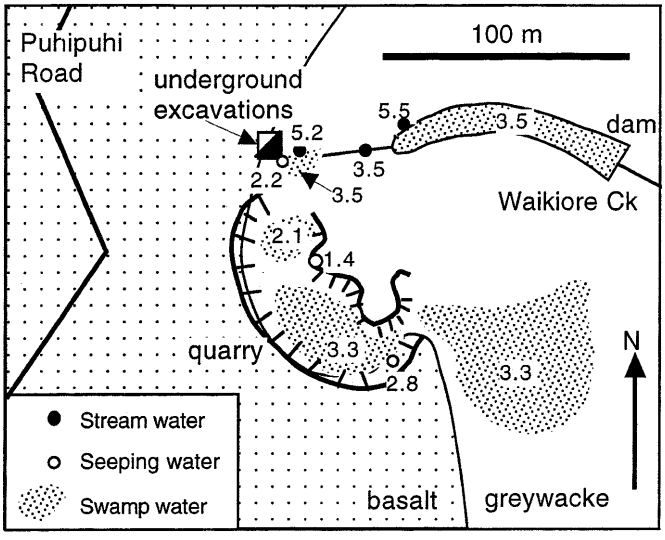

Fig. 4
Map of the Hg Mine at Puhipuhi (Fig. 2; after Henderson 1944) showing the main workings (quarry) in relation to surface water distribution. Measured pH of surface waters are indicated, as swamp (*stippled*), flowing stream (*black circle* at sample point), or seep emanating from rock (*open circle* at sample point)

to 23 m thick occurs across an area of 600 × 400 m (Grieve and others 1997). The sinter consists of cryptocrystalline silica bedded on a 0.1–1 cm scale. Some of the silica has undergone post-depositional recrystallization, obscuring the finer features of bedding. The sinter is well exposed in a quarry which has been recently blasted, so fresh samples are available.

The Hg Mine (Figs. 2, 4) was developed in brecciated Mesozoic chert at the contact between basement and overly-

ing basalt (Henderson 1944; White 1986). The mineralized zone is about 200 m wide and consists of highly silicified brecciated host rock weakly cemented by cinnabar, silica, pyrite, and kaolinite. The mine consisted of an open cut quarry (Fig. 4) and some small underground workings (Henderson 1944), all of which are now extensively overgrown with regenerating vegetation. Outcrops at the quarry are still preserved, and mine waters lie on the quarry floor and emanate from underground excavations. Oxidized rock on the margins of the mine, and in fragments on the quarry, is locally impregnated and cemented with limonite formed from pyrite oxidation. Extensively mineralized basement greywackes and argillites are exposed in a now abandoned quarry at the north end of Puhipuhi Road (Fig. 2). These basement rocks are cut by irregular veins (0.1–10 mm wide) of quartz, cryptocrystalline silica, and kaolinite with abundant sulfides, mainly marcasite. Adjacent host rock is variably hydrothermally altered into clays, particularly kaolinite. Locally, the host rock is intensely silicified and impregnated with cinnabar and iron sulfides.

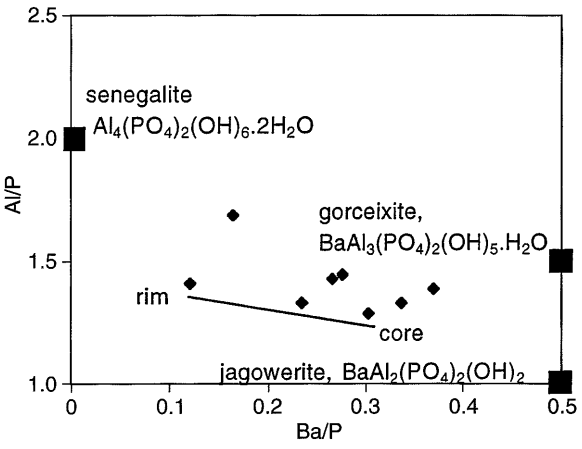

Fig. 5
Chemical composition of barium phosphate minerals (*black diamonds*) from the Puhipuhi quarry (Fig. 2, Table 2) as determined by microprobe analysis. Compositions are recalculated from wt% oxides to atomic proportions, and expressed as ratios to facilitate comparison to ideal formulae, as indicated in the diagram (*black squares*)

Principal metal-bearing minerals

The principal mercury- and arsenic-bearing minerals at the various levels in the composite hydrothermal systems (Fig. 3) are summarized in Table 1.

Cinnabar (HgS) is a common, although volumetrically minor, constituent of many rocks in the Puhipuhi area. It occurs as trains of grains up to 1 mm but generally <100 μm across in cryptocrystalline quartz, imparting a deep red colour to some layers in fresh exposures. Over weeks to years this red colour fades to grey in sunlight. Typical mercury ore at the Hg Mine was ca. 1% cinnabar (Henderson 1944). Other localities have lower concentrations.

Pyrite and marcasite (FeS_2) are common as accessory minerals in hydrothermally altered rocks in the Puhipuhi area, particularly at the Hg Mine (pyrite) and the Puhipuhi quarry (marcasite). Red layers in sinter at Mt. Mitchell contain cinnabar and pyrite, with the sulfides forming up to 20% of the layers. Associated black layers contain pyrite only. Post-depositional marcasite forms radiating clusters of elongate crystals up to 1 cm across on fracture surfaces and in cavities in the Mt. Mitchell sinter.

These iron sulfides readily oxidize at surfaces exposed to the atmosphere, yielding brown iron oxyhydroxide coatings on outcrops or iron oxyhydroxide cements to sediments in the immediate vicinity. Clusters of micron-scale FeS grains, probably mackinawite, occur on the outer margins of some marcasite crystals at the Puhipuhi quarry and may be a secondary feature formed from surficial recrystallization of marcasite.

Two distinctive metallic phosphate minerals have been identified optically and by microprobe at the Puhipuhi quarry: Ba-rich phosphate and Sc-rich phosphate. The Ba-rich phosphate, the most common, occurs as scattered grains and in veinlets up to 50 μm across (Fig. 5). Grains are typically euhedral to subhedral with a hexagonal cross section and are commonly zoned with darker cores

Table 1
List of the most important mercury and arsenic minerals at the localities discussed in the text, and their relative solubility under the prevailing surficial chemical conditions

Locality	Mineral	Hg, As abundance	Mineral abundance	Solubility
Ngawha	Native mercury	Pure Hg	Common	Low
	Cinnabar	HgS, minor As	Common	Very low
Mt. Mitchell	Cinnabar	HgS, minor As	Common	Very low
	Marcasite	up to 1 wt% Hg, As	Common	High
Hg Mine	Cinnabar	HgS, minor As	Common	Very low
	Marcasite	Up to 1 wt% Hg, As	Common	High
	Cinnabar	HgS, minor As	Rare	Very low
Puhipuhi quarry	Marcasite	Up to 1 wt% Hg, As	Very common	High
	Mackinawite	Up to 1 wt% Hg, As	Rare	Very high
	Ba-phosphate	Up to 0.5 wt% Hg, As	Common	Moderate-high

Table 2
Microprobe analyses (wt%) of phosphate minerals from the Puhipuhi quarry

	Barium phosphates								Scandium phosphates	
			Rim	Centre						
P_2O_3	22.16	21.73	24.97	24.09	20.54	24.23	23.11	22.74	31.73	21.19
BaO	17.09	9.56	8.40	20.35	15.17	15.77	23.77	21.44	7.74	5.55
SiO_2	0.35	1.40	0.00	0.03	2.47	2.67	2.70	0.26	12.39	23.79
CaO	2.98	3.54	5.50	2.69	1.81	3.35	1.65	1.62	0.18	0.10
Al_2O_3	29.75	32.97	32.74	28.82	27.21	29.88	29.60	27.96	10.19	19.56
K_2O	0.55	0.89	0.35	0.14	0.03	0.12	0.02	0.00	0.00	0.13
FeO	0.81	1.12	1.06	0.95	0.69	1.02	1.36	0.74	1.18	0.94
Sc_2O_3	0.17	0.00	0.06	0.00	0.00	0.00	0.00	0.00	31.52	21.21
Total	73.87	71.20	73.07	77.06	67.92	77.05	82.21	74.76	94.92	92.47
Cation										
P	2.404	2.246	2.500	2.576	2.358	2.439	2.342	2.536	2.473	1.567
Ba	0.664	0.354	0.302	0.780	0.624	0.569	0.864	0.857	0.216	0.147
Si	0.035	0.132	0.000	0.003	0.260	0.246	0.250	0.026	0.884	1.610
Ca	0.316	0.358	0.540	0.282	0.204	0.331	0.163	0.178	0.014	0.007
Al	3.479	3.674	3.534	3.322	3.369	3.242	3.235	3.363	0.856	1.560
K	0.070	0.107	0.040	0.017	0.004	0.015	0.002	0.000	0.000	0.011
Fe	0.067	0.089	0.081	0.078	0.061	0.079	0.106	0.064	0.070	0.053
Sc	0.015	0.000	0.004	0.000	0.000	0.000	0.000	0.000	1.959	1.251
Total	7.051	6.961	7.001	7.057	6.879	6.920	6.963	7.024	6.472	6.206

and lighter rims. Microprobe analyses show that the Ba content varies from 8 to 24 wt% within and between grains. Ba content varies antithetically with Al content (Table 2; Fig. 5), while phosphate content remains approximately constant. The scale of zoning in individual grains, together with the small grain size and consequent overlap onto neighbouring minerals, ensures that all microprobe analyses are composite. Analyses obtained suggest that some solid solution may exist between senegalite and jagowerite (Fig. 5).

The Sc-bearing phosphate occurs as rare scattered grains (5–20 μm) in kaolinite pools and veinlets. These phosphate grains mainly yield composite analyses with enclosing minerals, mainly quartz (Table 2), due to their fine grain size, but most analyses are consistent with a mineral formula of $ScPO_4 \cdot 2H_2O$, kolbeckite.

Mercury and arsenic in mineralized zones

Methods

Detailed investigations of arsenic and mercury distributions were carried out using microprobe mapping techniques on a JEOL 8600 microprobe. Microprobe maps were constructed using automated analysis of 2-μm diameter spots on a 2-μm grid pattern over selected areas of polished thin sections. Each spot analysis results from 0.1-s counting, using wavelength dispersion at 25 kV. Background As and Hg levels vary from mineral to mineral and are highest over metallic minerals, approaching 0.5 wt% As or Hg. Hence, the detection limit for As and Hg is ca. 0.5 wt% under these conditions, and results close to, but above this limit are semiquantitative only. Resolution of anomalous concentrations of As and Hg near this detection limit is difficult.

Four types of material were examined in detail by microprobe mapping: Mt. Mitchell sinter; unoxidized silicified greywacke from the Hg Mine; oxidized kaolinitized greywacke from the Hg Mine; and kaolinitized and silicified argillite from the Puhipuhi quarry. These samples give a representative view of the main types of material found in the Puhipuhi area. Maps were constructed of portions of these samples. They show the most variations in overall mineralogy and metal contents through the different levels of the Puhipuhi fossil hot spring systems. Examples from the resulting maps are presented in Figs. 6 and 8. More detailed Hg and As maps of a smaller area of Fig. 8 were produced using 1-s counting time and 1-μm analysis grid. The resulting maps are poorly resolved, but interpretations have been incorporated into Fig. 9.

Mt. Mitchell sinter

The Mt. Mitchell sinter material examined in detail consists almost entirely of quartz with disseminated pyrite crystals (up to 20 μm). Micron-scale pyrite grains are barely discernable in the iron map (Fig. 6a), scattered irregularly through the quartz. Thin (10–30-μm) layers rich in micron-scale cinnabar crystals trace tortuous paths through the quartz (Fig. 6d). These represent primary layers in the sinter distorted by surficial slumping processes during formation.

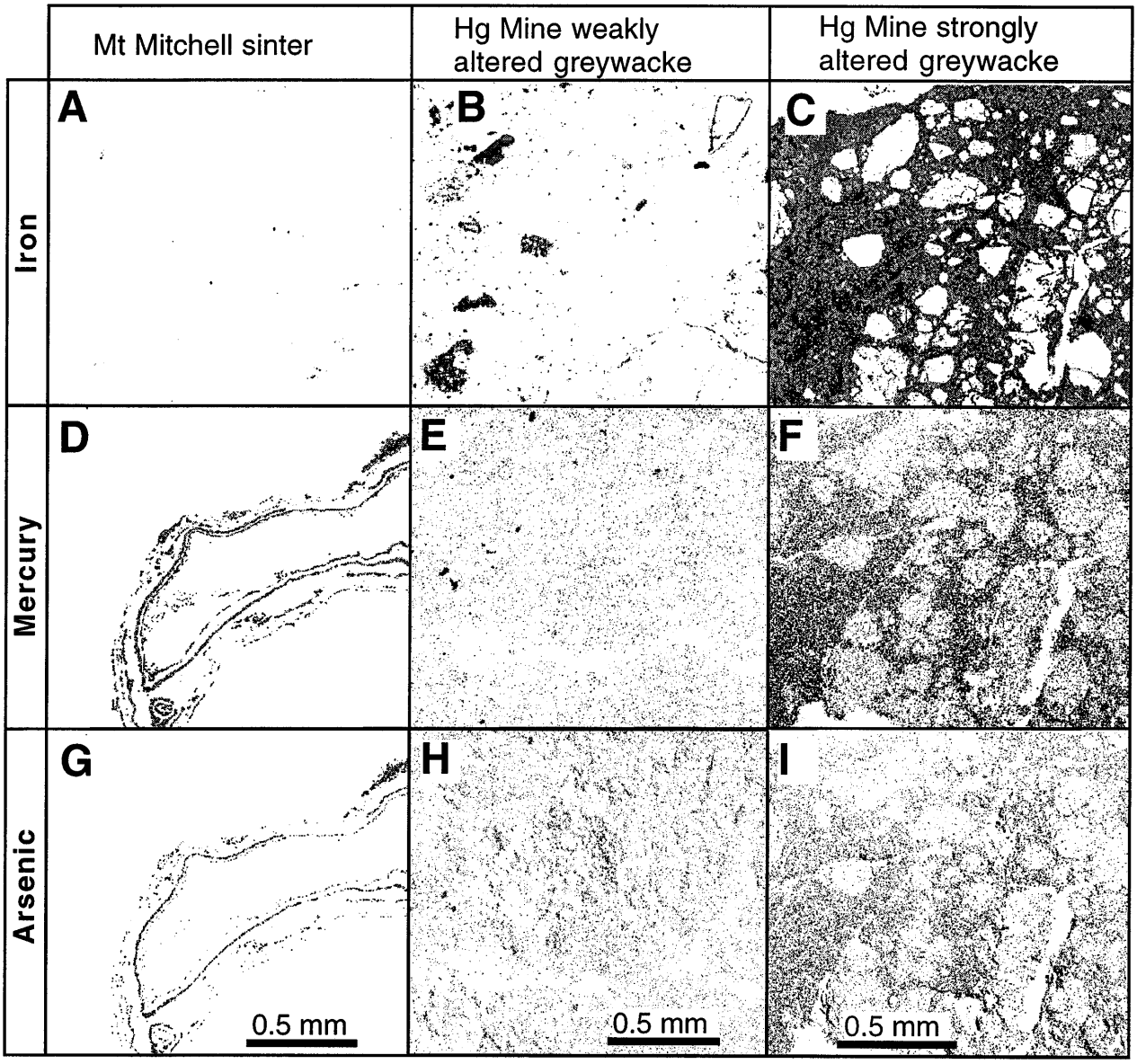

Fig. 6
Microprobe element maps (see text for descriptions of mapping techniques) of Mt. Mitchell sinter (**a**, **d, g**), weakly altered greywacke from the Hg Mine (**b, e, h**), and strongly altered and oxidized greywacke from the Hg Mine (**c, f, i**). The maps are arranged for comparison of iron maps (**a, b, c**), mercury maps (**d, e, f**), and arsenic maps (**g, h, i**) among the three different types of material

The arsenic pattern on the microprobe map (Fig. 6g) follows the mercury pattern (Fig. 6d) exactly, and is a result of an elevated As background over the Hg-bearing cinnabar. Hence, this map is essentially a microprobe artifact and is presented for comparison to other As maps showing genuine anomalies. Nevertheless, the sinter material contains As levels up to 40 ppm, as determined by XRF analyses. This As is at least partly in solid solution in the cinnabar, but at levels well below microprobe detection.

Hg Mine

Two samples were selected: one grey and weakly altered from the south end of the mine quarry (Fig. 4); and one brown (oxidized) and highly altered from the main mine area. Both samples consist of fragments of varying grain size from the Hg Mine floor sediment, and the fragments are detritus from typical outcrops in the mine. The fragments consist predominantly of variable amounts of quartz and kaolinite from the mineralized hydrothermally altered zone. Microprobe element maps were constructed of a portion of a typical rock fragment from each of these two sediment samples.

Mercury distribution

The grey and weakly altered specimen is dominated by quartz, with subordinate kaolinite and minor scattered iron sulfides. The sulfides are small (<50 μm), showing up as black patches in the iron map (Fig. 6b; e.g., near

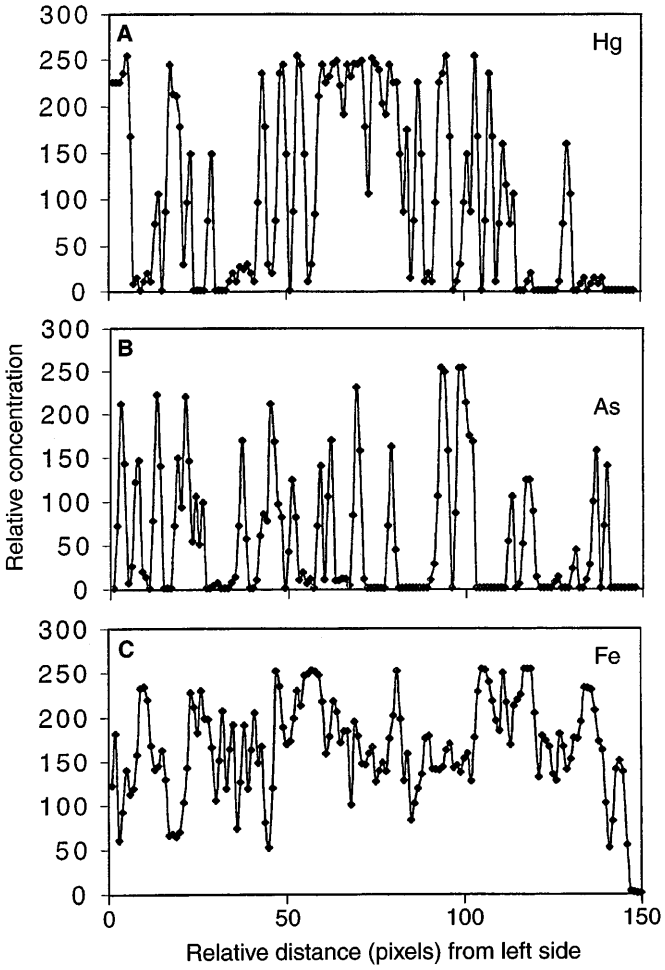

Fig. 7
Semiquantitative element profiles horizontally across a portion of the lower left of element maps in Fig. 6c, f, i (see text), showing relative intensities of element signals across the profiles. Vertical scale places all data between zero and 250 arbitrary units, with background for Hg and As ca. 50–100 of these units, and Fe background near zero units. **a** Mercury profile showing localized high Hg zones, especially in the middle of the profile; **b** arsenic profile, with scattered small high-concentration zones; **c** iron profile, with variable but moderate iron contents throughout

top right). Some scattered fine-grained cinnabar also occurs (Fig. 6e, prominent black spots). The grain sizes and shapes in the rest of the rock are indicated by localized limonite staining of grains (Fig. 6b). As it was constructed to detect low levels of Hg near to detection limit, the Hg map (Fig. 6e) shows mainly background (palest patterns) rather than any true signal. Other than in the sulfides, localized diffuse but darker patches show relatively high Hg , suggesting that there is dispersed Hg in kaolinite at marginally detectable levels (ca. 0.5 wt%). The brown altered material from the main Hg Mine area yields a set of maps which show more textural and chemical detail than the grey material (Fig. 6c,f,i). Quartz grains within the mapped fragment show up as clear or low-density zones , defining the rock texture of scattered quartz grains surrounded by other silicate material, mainly kaolinite. No sulfides were detected. The kaolinite is intensely stained and impregnated with limonite (Fig. 6c). Mercury (Fig. 6f) has higher background over these iron oxyhydroxide-rich zones (Fig. 6c) than over quartz, accounting for some of the variation in mercury distribution. However, localized dark zones in the mercury map (Fig. 6f; e.g., lower left) represent zones generally enriched in mercury at low levels ($<1\%$). The mercury appears to be associated with limonite and may be co-precipitated with limonite (Hem 1977). However, semi-quantitative examination of mercury-rich zones in Fig. 6f show that high mercury is not directly correlated with high iron (Fig. 7a,c). These profiles were constructed along a ca. 300-μm horizontal line in the lower left of the Fig. 6 maps, 120 μm from the base line. The vertical axes in these profiles display only relative differences in element concentrations, with an arbitrary scale between 0 and 250. The most prominent mercury anomaly, in the centre of the profile (Fig. 7a), coincides with only moderate iron concentrations (Fig. 7c), and higher iron concentrations on either side of this zone have very variable Hg concentrations. It is not possible to determine the exact mineralogical nature of the mercury concentrations in this material because of the extremely fine grain size and complex admixture with other minerals.

Arsenic distribution

Arsenic distribution in Hg Mine material is similar to that of mercury , and As occurs in localized concentrations in the Hg Mine maps (Fig. 6h,i). In the weakly altered grey material from the south end of the Hg Mine, As occurs locally with limonite (Fig. 6h, top right and centre), but is mainly in diffuse zones distributed through the kaolinite. The general association of arsenic with limonite is stronger in the brown altered material from the main part of the Hg Mine where As concentrations occur around the margins of quartz grains in iron-stained kaolinite (Fig. 6i; e.g., lower right). However, in detail there is no direct correlation between iron concentration and arsenic concentration (Fig. 7b,c).

Puhipuhi quarry

Microprobe maps were constructed of a representative section across the margin of a mineralized vein cutting hydrothermally altered argillite and greywacke from the Puhipuhi quarry (Fig. 8). The geometry and texture of the vein are indicated by the sulfur map (Fig. 8a), showing marcasite crystals protruding from the left into an open cavity. An associated phosphate-rich vein is defined by barium (Fig. 8b) at the base of the maps, in conjunction with quartz vein material. Detailed As and Hg distributions of a small portion of these maps (box in Fig. 8a) are summarized in Fig. 9.

Arsenic distribution

Arsenic content of altered rocks at the Puhipuhi quarry, as determined by XRF analysis, ranges from 7 to 30 ppm and is highest in marcasite-rich material. Distribution of

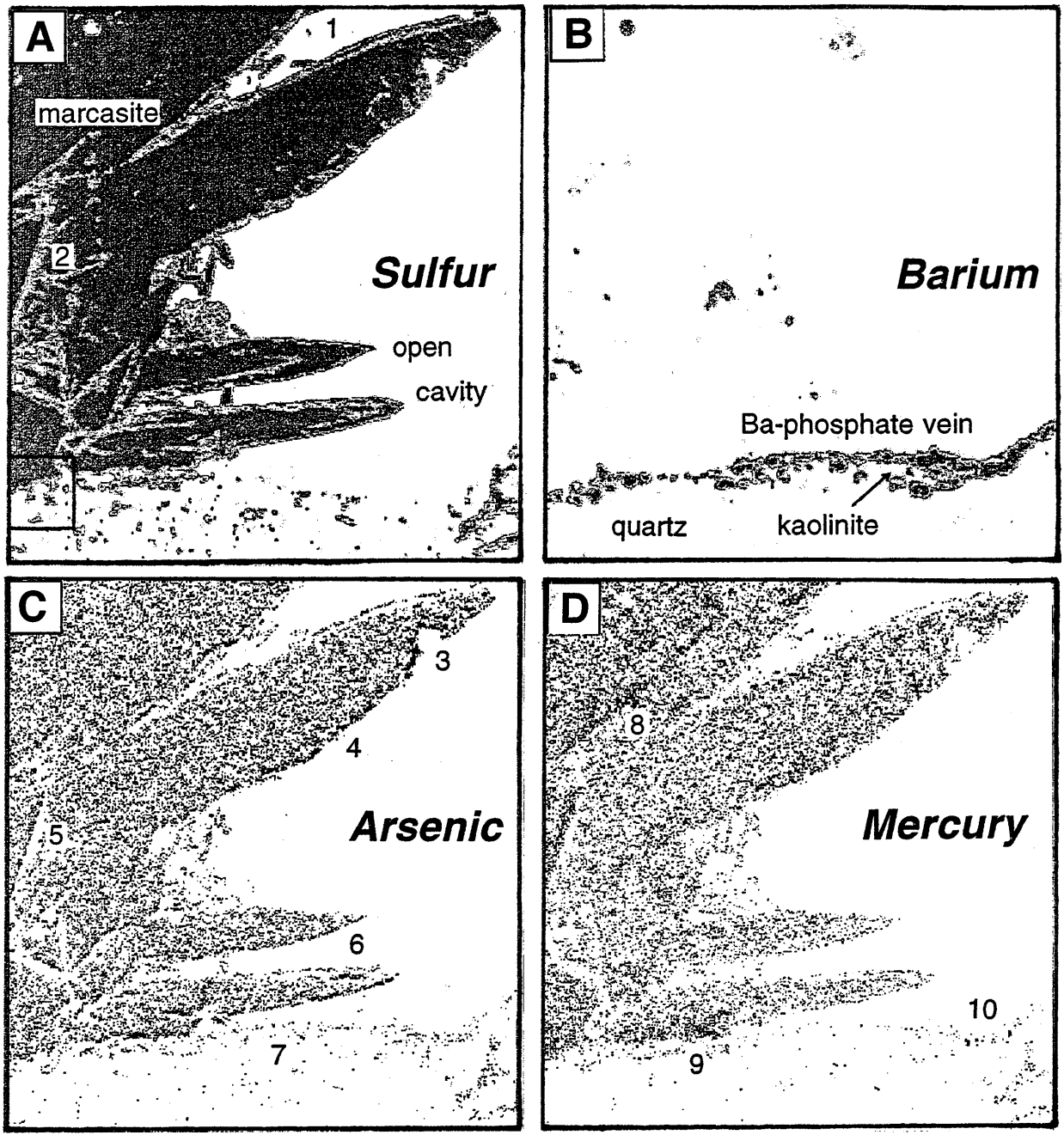

Fig. 8
Microprobe element maps of a marcasite-bearing vein in hydrothermally altered basement rock from the Puhipuhi quarry. All maps (**a–d**) are of exactly the same area of a thin section, and the horizontal field of view in each map is 0.8 mm. The *dark feature* on the left of map **a** is a cluster of marcasite crystals shown up by their high sulfur content. Arsenic and mercury contents are indicated in maps **c** and **d** respectively, although much of the As and Hg signature is background and confirmed As and Hg enrichment occurs only at relatively dark parts of the maps, principally on crystal edges. *Numbers* on the maps refer to points discussed in the text. A barium phosphate vein is shown in the Ba map (**b**). *Box* in lower left of **a** (100 μm across) shows the area mapped in Fig. 9

arsenic in the marcasite-rich mapped sample is depicted by the microprobe map in Fig. 8c. The arsenic is concentrated along the outer margins of marcasite crystals (e.g., between points 3 and 4, and the mineral grain at point 6, in Fig. 8c). Similar concentrations occur at crystal margins within marcasite masses (e.g., point 5 in Fig. 8c). A localized concentration of As at point 3 (Fig. 8c) is in an Fe-S mineral, probably mackinawite (above), on the marcasite margin. The As in marcasite is irregularly distributed on the 100-μm scale on crystal margins (Fig. 9). Arsenic is also irregularly distributed through the Ba-phosphates, as shown in the vein in Fig. 8b,c. The As is concentrated principally in Ba-phosphate grains on the upper edge of that vein (see point 7, Fig. 6c). There is a

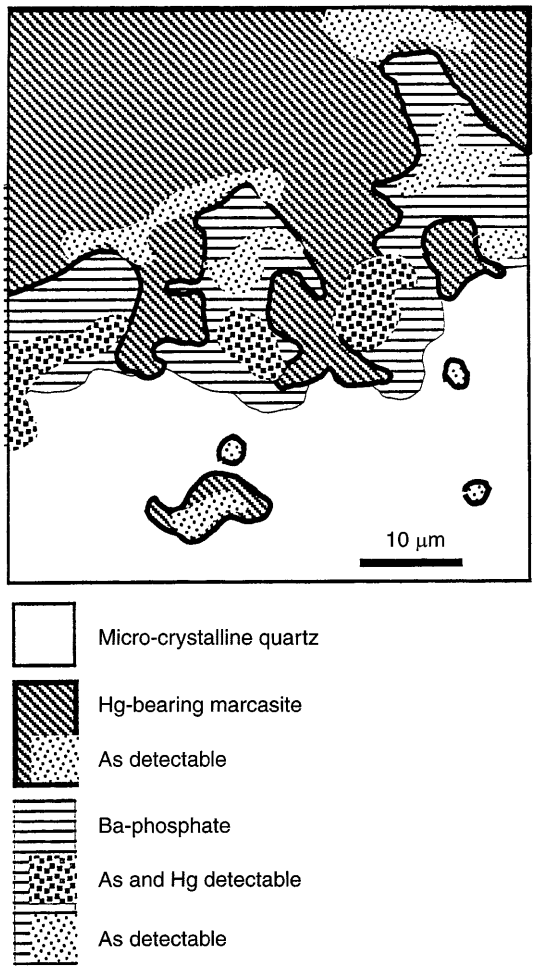

Fig. 9
Generalized microprobe map of the detailed area indicated in Fig. 8a, on the edge of marcasite crystals (*top*) with a zone of fine-grained Ba-phosphate minerals (*centre*) between the marcasite and quartz (*bottom*). Hg and As contents of the marcasite and phosphates are variable, as indicated by different *shading*. Detectable As and Hg is >0.5 wt%. The map was drawn from a microprobe map generated in the same way as described for Fig. 6, but resolution is poorer at this scale

patchy distribution of As in Ba-phosphate at the 100-μm scale near marcasite grain margins (Fig. 9).

Mercury distribution

Distribution of mercury in marcasite from Puhipuhi quarry is similar to that of arsenic, but more diffuse. Concentrations of Hg near marcasite grain margins occur in broader zones than arsenic (e.g., points 8 and 9, Fig. 8d). A Hg-rich marcasite zone near point 9 (Fig. 8d) extends left into a marcasite cluster in which all marcasite has detectable Hg (Figs. 8d, 9). Some of this Hg-rich marcasite also contains detectable As, but some Hg alone (Fig. 9).
Mercury is also detectable in some portions of the Ba-phosphates, such as near point 10 (Fig. 8d). This region of the Ba-phosphate vein is also most enriched in arsenic (Fig. 8c). However, mercury distribution in the Ba-phosphates is patchy, and detectable Hg can occur with or without associated detectable As (Fig. 9).

Geochemical environment

The geochemical environment can be conveniently expressed in terms of the acidity and oxidation state of surficial waters in contact with the deposits. These parameters can be quantified in the field by measuring pH (hydrogen ion concentration) and Eh (relative redox state with respect to the hydrogen electrode). These data were collected using an Oakton WD35615 portable meter with a combination pH and Eh electrode. Data can be recorded digitally to two decimal places and are reproducible to ca. 0.2 pH units and ca.10 mV.
Results of pH and Eh measurements in surface waters and wet soils from the study's three sites are depicted in Fig. 8a-d. A sketch map of the Hg Mine (Fig. 4) shows measurement points for that locality and the variation of pH in the area. Background stream pH is between 6 and 7.5 in the Puhipuhi area. Downstream (ca. 200 m) from the Hg Mine, the Waikiore Stream (Fig. 4) has a pH within this background range. However, the pH is distinctly lower than this in the immediate vicinity of the mine workings, especially in seepages from the quarry walls (Fig. 4). Likewise, damp soils and surface seeps in the Mt. Mitchell quarry are similarly acid (Fig. 10a). Seeps emanating from the Puhipuhi quarry have a very low pH, down to ca. 1 (Fig. 10a).
These observed data define a spread ranging from poorly oxygenated waters with near-neutral pH in the more distal areas of the deposits to relatively reduced acid waters in the vicinity of the Puhipuhi quarry (Fig. 10a). The data fall outside the stability field for limonite and mainly cluster near the stability boundary of pyrite (and/or marcasite) (Fig. 10a). Limonite stains occur on the margins of swamps and on quarry walls at the Hg Mine. These deposits may be due to the oxidation of dominantly ferrous iron-bearing mine waters depicted in Fig. 10a.
The measured values of pH and Eh suggest that dissolved sulfur occurs principally as sulfate ions (Fig. 10b). The more acid waters emanating from the Puhipuhi quarry are theoretically in equilibrium with crystalline elemental sulfur (Fig. 10b). No sulfur has been confirmed in any samples examined in this study, but yellow sulfur-looking stains occur on some rock surfaces. Sulfur in the surficial environment of the studied deposits is derived by oxidation of iron sulfides, mainly marcasite and pyrite:

$$FeS_2 + 7/2O_2 + H_2O = 2SO_4^{2-} + Fe^{2+} + 2H^+$$

(Garrels and Thompson 1960).
This equation implies that two sulfate ions and one ferrous ion are generated for each hydrogen ion. These relative proportions of ions are incorporated into construction of the Eh-pH diagrams in Fig. 10a-d, with dissolved sulfur concentrations increasing with decreasing pH (Fig. 10b).

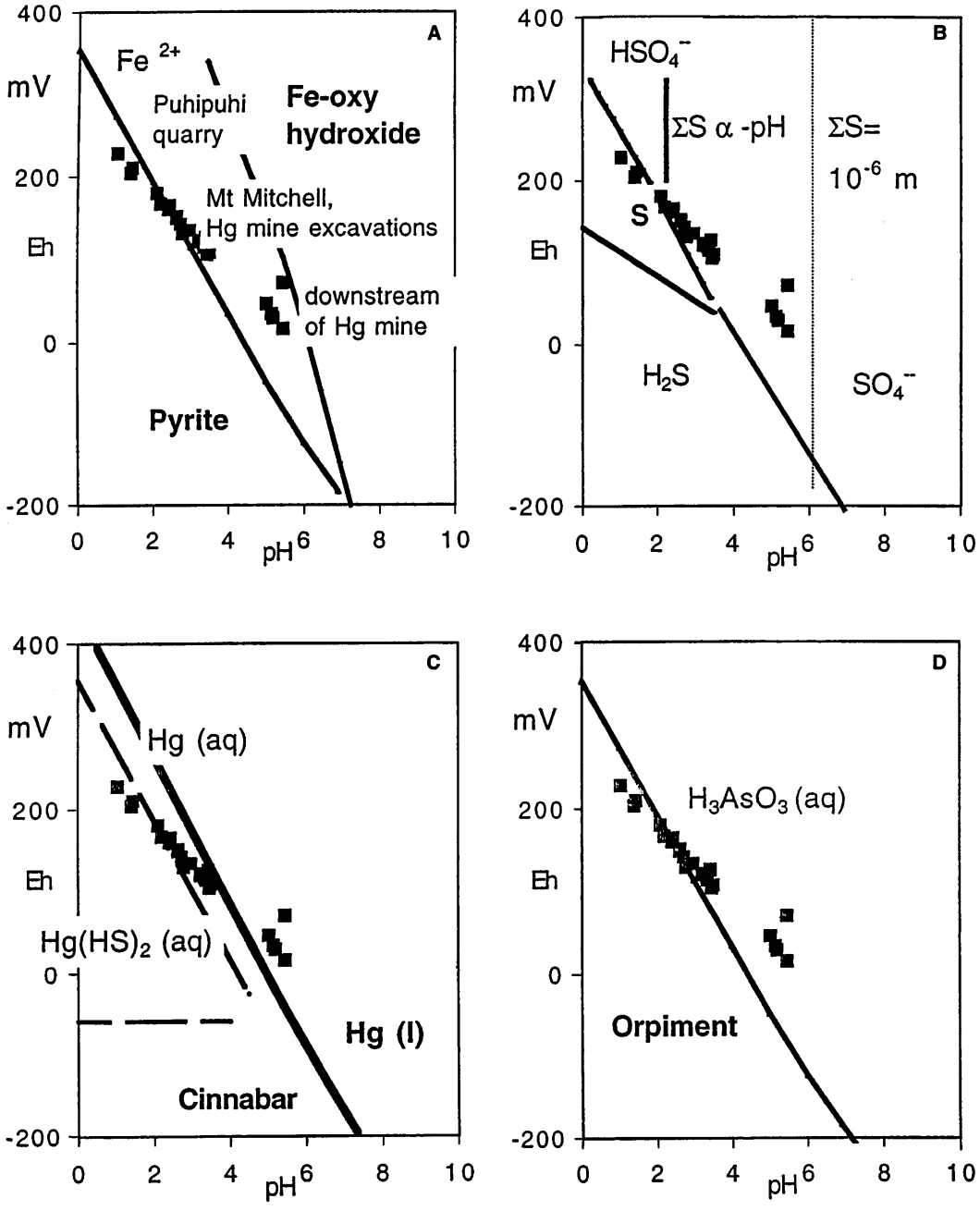

Fig. 10
Geochemical diagrams depicting pH and redox potential (Eh) of the surficial environment measured in the Puhipuhi area (*black squares*). Sites at which data were collected are indicated in **a**, along with relative stabilities of iron minerals (*bold lettering*) and aqueous ferrous iron. Dominant sulfur species boundaries are indicated in **b**. Relative stabilities of mercury and arsenic minerals (*bold lettering*) and predominant aqueous species are shown in **c** and **d** respectively. Boundaries were drawn from data in Garrels and Christ (1965), Hem (1970), and Webster (1990), assuming solution composition is dominated by pyrite/marcasite decomposition (Fig. 11)

Environmental availability of Hg and As

Theoretical Hg and As mobility

Marcasite is volumetrically the most important metalliferous mineral which decomposes in the studied deposits, and decomposition of this marcasite dominates the geochemistry of waters emanating from the deposits. Marcasite is stable under surficial reducing conditions (Schoonen and Barnes 1991), but is a relatively unstable mineral under oxidizing conditions, compared to pyrite, and readily decomposes. The rate of decomposition varies with grain size and crystallinity, but clean crystalline

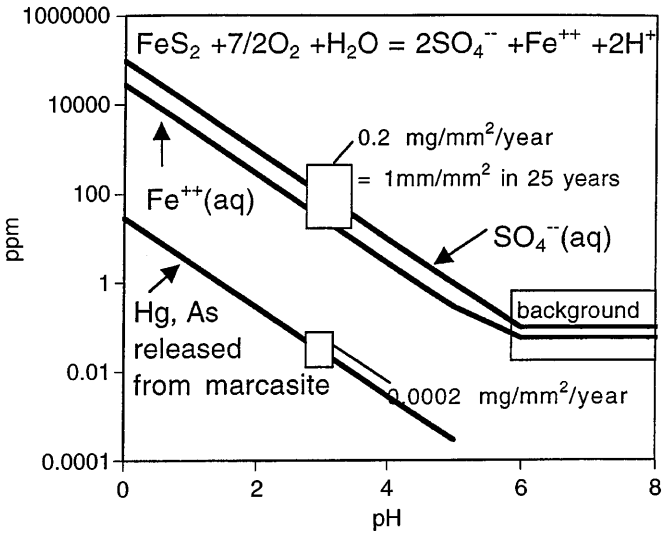

Fig. 11
Theoretical solution concentrations which result from decomposition of pyrite or marcasite via the equation at the *top* of the diagram (Garrels and Thompson 1960). The *top two lines* are for dissolved sulfate and ferrous iron, as indicated. Mercury and arsenic released from marcasite such as at Puhipuhi quarry will have concentrations as indicated by the *lower line*. Experimental marcasite decomposition rate (Rinker and others 1997) and its effects on As and Hg release at Puhipuhi are indicated by *boxes* at pH 3

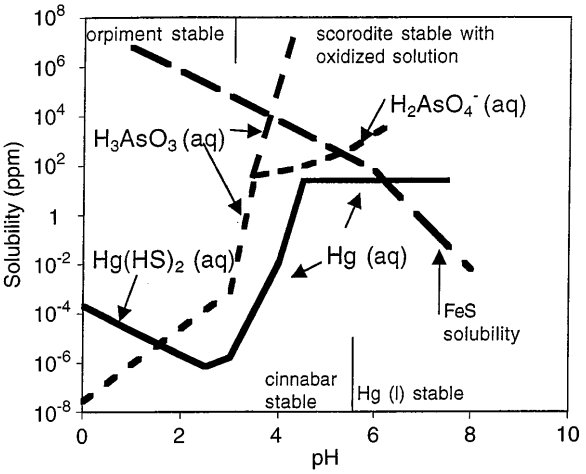

Fig. 12
Theoretical solubilities of arsenic (*short dashed lines*) and mercury (*solid lines*) under the chemical conditions derived from field measurements at Puhipuhi (Fig. 10). Principal aqueous species are indicated by *small letters*. Mackinawite solubility, releasing As and Hg, is shown by *long dashes*. Sources are outlined in the text

marcasite decomposes at a rate of about 0.2 mg mm^{-2} $year^{-1}$ at pH 3 (Rinker and others 1997). This is equivalent to decomposition of a 1 mm thickness of exposed marcasite surface in 25 years (Fig. 11). Chemical consequences of marcasite decomposition are depicted in Fig. 11.

Marcasite crystals in the Puhipuhi quarry locally contain up to 0.8 wt% Hg and As (Fig. 8c,d). These heavy metals are irregularly distributed in what appears to be a diffuse manner, so it is assumed that the metals are present in solid solution in the marcasite rather than as separate mineral grains. Elsewhere in the same marcasite crystals the Hg and As contents are below microprobe detection limits (ca. 0.5 wt%) but are unlikely to be zero if the metals are present in solid solution. A conservative estimate of 0.1 wt% Hg and As in solid solution in marcasite is plausible. This Hg and As will be released as the marcasite decomposes, as depicted in Fig. 11. The rate of Hg and As release is directly related to the rate of decomposition of marcasite: ca. 0.0002 mg Hg or As mm^{-2} $year^{-1}$ at pH 3 (Fig. 11).

Release of Hg and As from marcasite does not necessarily imply that these metals will remain in solution. Solubility of Hg is very low under the low pH conditions of marcasite decomposition (Fig. 12). In the cinnabar stability field, mercury can go into solution as $Hg(HS)_2$ (aq) or Hg (aq) (Hem 1970; Figs. 10c, 12). For the chemical conditions inferred for the Puhipuhi quarry (Fig. 10a), mercury solubility is generally less than 1 ppb (Fig. 12). At higher pH, mercury exists as elemental liquid and Hg (aq), and solubility is ca. 25 ppb (Hem 1970; Figs. 10c, 12). We have no observational evidence of surficial formation of either cinnabar or liquid Hg, but their presence should be expected where marcasite is decomposing – unless sufficient surface water flushing can remove all the released mercury at low concentrations (sub-ppb level).

Arsenic is also insoluble at low pH under chemical conditions governed by marcasite decomposition, and orpiment (As_2S_3) is the stable arsenic mineral in the Puhipuhi quarry below pH of 3 (Webster 1990; Fig. 10d). At higher pH, arsenic rapidly becomes soluble as As(III) ions (Vink 1996; Figs. 10d, 12). Hence, any As released by marcasite decomposition could be flushed out in solution by higher pH surface waters. We have no evidence of orpiment formation under surficial conditions in any of the Puhipuhi deposits, and complete flushing is suspected. Under more oxidizing conditions, As(III) ions become oxidized to As(V) ions, and scorodite ($FeAsO_4 \cdot 2H_2O$) controls the amount of As in solution (Krause and Ettel 1988; Fig. 12). Localized FeS minerals (mackinawite?) on the outside of marcasite grains contain As up to ca. 1 wt% but no detectable Hg (Fig. 10c,d). FeS mineral solubility increases with lowering pH (Morse and Arakaki 1993; Fig. 12), and the contained arsenic as well as any low levels of Hg will be released as the FeS minerals dissolve.

Cinnabar solubility is low under the observed chemical conditions (Fig. 12), and the kinetics of cinnabar dissolution ensure that little Hg should be released from this mineral. Cinnabar is widespread as a detrital mineral in many parts of the world, and has been reported as a detrital mineral in the Pliocene sediments at Puhipuhi (Ferrar 1925). These detrital occurrences suggest that cinna-

bar is resistant to chemical decay under oxidized and water-saturated conditions in the surficial sedimentary environment.
Solubility of Ba phosphates is not known, but most phosphates become more soluble with decreasing pH. However, metal-bearing phosphates have complex solubility behaviours and phosphates can even fix metals in the surficial environment (Melamed and Boas 1998; Sauve and others 1998; Valsami-Jones and others 1998). Consequently, it is not possible to predict the release of As and Hg from the Ba-phosphate material in the Puhipuhi quarry.

Experimental mobilization of mercury

To obtain some quantitative information on rates of metal release from Puhipuhi material, a set of leach experiments was conducted on a mineralized sample from the Puhipuhi quarry and some sediment samples from the floor of the Hg Mine quarry, at the north end, the main mine area, and the south end (Fig. 4). The Hg Mine samples included a range of material types, from clean grey quartz-rich material enclosing cinnabar from the north end and south end (as examined by microprobe, Fig. 6b,e,h) to friable brown limonite-stained clay-rich material (e.g., main mine area, Fig. 6c,f,i). Samples were divided into different subsamples because of sample inhomogeneity. Each subsample was crushed to fine powder in an agate mortar and subjected to leaching in sulfuric acid solutions for up to 18 days. Solutions with pH 3 and 1 and 50% sulfuric acid were used for these experiments to simulate acidic environments observed in the field (Fig. 10a). The leach solutions were analysed by Chemsearch (University of Otago Chemistry Department) with a detection limit of ca. 1 ppb for mercury.
Mercury leach results (Fig. 13) show that mercury concentrations in the pH 3 and 1 solutions generally decrease over time, from the analyses conducted in the first few days to the analyses conducted after more than a week, although some Hg Mine subsamples continued to release Hg at high levels. The amounts of Hg released from Puhipuhi quarry samples are relatively small at pH 3 and 1, generally less than 100 ppb (Fig. 13a,b). Nearly all Hg Mine subsamples released more Hg than the Puhipuhi quarry subsamples at pH 3 and 1, at levels up to 20 ppm. The 50% sulfuric acid solution leached variable but relatively large amounts of Hg from all samples, except those from the north end of the Hg Mine (Fig. 13c).
These leaching experiments show that small but possibly environmentally significant amounts of Hg can be leached from both cinnabar-rich and marcasite-rich localities under the typical acid conditions expected in old mine sites. The mineralogical differences between the studied sites become more important in strong acid where marcasite breaks down rapidly, releasing contained

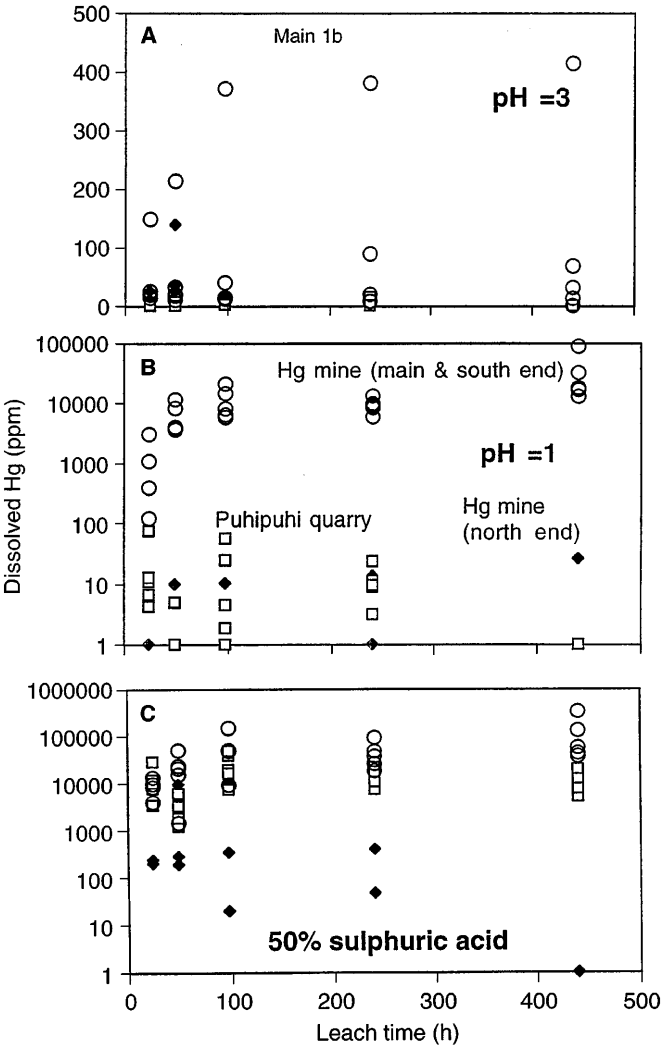

Fig. 13
Results of experimental leaching of mercury from samples from the Hg Mine (*black diamonds* north end; *open circles* main mine area and south end), and Puhipuhi quarry (*open squares*). Experiments used solutions with pH 3 (**a**), pH 1 (**b**), and 50% sulfuric acid (**c**). Note the log scale in **b** and **c**

Hg. The levels of Hg released from the Puhipuhi quarry material at pH 3 and 1 (10–100 ppb) are similar to those predicted from theoretical discussions on marcasite solubility (Fig. 11), and the increase in Hg released from marcasite with decreasing pH (Fig. 13) is in accordance with the theory (Fig. 11). Hg released from the Hg Mine material (Fig. 13) is greater than expected from the low theoretical solubility of cinnabar (Fig. 12). The cleanest cinnabar-bearing Hg Mine material (from the north end) yields the lowest Hg leach results (Fig. 13), and the highest leach results are for limonite-stained kaolinitic material (Fig. 6c,f,i). The dispersed mercury in the limonitic cement in that material is clearly loosely bound and easily removed in acid solutions.

Conclusion

Mercury and arsenic occur in a variety of minerals in the fossil hot springs in the Puhipuhi area. Cinnabar is the main mercury mineral in siliceous sinters formed at the paleosurface, and this material is relatively stable in the surficial environment. Cinnabar also occurs in variably altered rocks in the hot spring feeder zones beneath sinter deposits, and some of this cinnabar may be leached by surficial solutions. Lower but environmentally more significant Hg levels occur in marcasite and phosphate minerals locally in excess of 0.5 wt%, and dispersed in limonite cements at >0.5%. These latter minerals can release Hg into the environment more readily than coexisting cinnabar which is relatively insoluble. Likewise, arsenic occurs in marcasite and phosphate minerals and is dispersed through limonite, locally in excess of 0.5 wt%, and can be released into the environment as these minerals decompose under surficial oxidizing acid conditions. The amount of As and Hg released is linked to the solubility of the host minerals, and generally increases with decreasing pH. The pH of the Puhipuhi fossil hot spring feeder zones is commonly acid (pH as low as 2) due to decomposition of iron sulfides which accompanied primary mineralization, and this acidity enhances release of Hg and As into the environment.

Acknowledgements The research upon which this report is based was funded by the NZ Government Public Good Science Fund via Contract UOO620. Additional information was kindly provided by the Northland Regional Council, Dr. Jenny Webster, and Peter Grieve of Delta Gold NZ Ltd. Experimental leaching studies were carried out by Frank Ho of Chemsearch, and we are grateful for his enthusiasm. Damien Walls provided XRF arsenic analyses of selected material, and Brent Pooley provided thin sections of extremely difficult material. Hospitality of the faculty and staff of the Colorado School of Mines during preparation of this paper was much appreciated.

References

Axtmann RC (1975) Environmental impact of a geothermal power plant. Science 187:795–797

Baldi F (1988) Mercury pollution in the soil and mosses around a geothermal power plant. Water Air Soil Pollut 38:111–121

Ferrar HT (1925) Geology of the Whangarei-Bay of Islands Subdivision. NZ Geol Survey Bull 27

Ferrara R, Maserti BE, Breder R (1991) Mercury in abiotic and biotic compartments of an area affected by a geochemical anomaly (Mt Amiata, Italy). Water Air Soil Pollut 56:219–232

Garrels RM, Christ CL (1965) Solutions, minerals and equilibria. Harper and Row, New York

Garrels RM, Thompson ME (1960) Oxidation of pyrite in iron sulfate solutions. Am J Sci 258A:57–67

Grieve PL, Corbett GJ, Leach TM (1997) Geology and exploration at Puhipuhi, Northland, New Zealand. Proc NZ Minerals and Mining Conf, Ministry of Commerce, Wellington, NZ, pp 133–139

Hem JD (1970) Chemical behaviour of mercury in aqueous media. USGS Prof Pap 713:19–24

Hem JD (1977) Reactions of metal ions at surfaces of hydrous iron oxide. Geochim Cosmochim Acta 41:527–538

Henderson J (1944) Cinnabar at Puhipuhi and Ngawha, North Auckland. NZ J Sci Technol 26:47–60

Kear D, Hay RF (1961) Sheet 1:North Cape. Geol Map of NZ 1:250 000. Dept Sci Ind Res, Wellington

Krause E, Ettel VA (1988) Solubility and stability of scorodite, $FeAsO_4 \cdot 2H_2O$: new data and further discussion. Am Mineral 73:850–854

Loebenstein JR (1993) Arsenic: supply, demand and the environment. In: Mercury and arsenic wastes: removal, recovery, treatment and disposal. US EPA Pollut Tech Rev 214:67–71

Melamed R, Boas RCV (1998) Phosphate-background electrolyte interaction affecting the transport of mercury through a Brazilian oxisol. Sci Total Environ 213:151–156

Morse JW, Arakaki T (1993) Adsorption and coprecipitation of divalent metals with mackinawite (FeS). Geochim Cosmochim Acta 57:3635–3640

Rinker MJ, Nesbitt HW, Pratt AR (1997) Marcasite oxidation in low-temperature acidic (pH 3.0) solutions: mechanism and rate laws. Am Mineral 82:900–912

Sauve S, McBride M, Hendershot W (1998) Lead phosphate solubility in water and soil suspensions. Environ Sci Technol 32:388–393

Schoonen MAA, Barnes HL (1991) Reactions forming pyrite and marcasite from solution. 1 Nucleation of FeS2 below 100 °C. Geochim Cosmochim Acta 55:1495–1504

Smith IE, Okada T, Itaya T, Black PM (1993) Age relationships and tectonic implications of late Cenozoic basaltic volcanism in Northland, New Zealand. NZ J Geol Geophys 36:385–393

Turner RR (1993) Effect of chemical form of mercury on the performance of dosed soils in standard leaching tests: EP and TCLP(1). In: Mercury and arsenic wastes: removal, recovery, treatment and disposal. US EPA Pollut Tech Rev 214:14–18

Valsami-Jones E, Ragnarsdottir KV, Putnis A, Bosbach D, Kemp AJ, Cressey G (1998) The dissolution of apatite in the presence of aqueous cations at pH 2–7. Chem Geol 151:215–233

Varekamp JC, Buseck PR (1983) Hg anomalies in soils: a geochemical exploration method for geothermal areas. Geothermics 12:29–38

Vink BW (1996) Stability relations of antimony and arsenic compounds in the light of revised and extended Eh-pH diagrams. Chem Geol 130:21–30

Webster JG (1990) The solubility of As2S3 and speciation of As in dilute and sulphide-bearing fluids at 25 and 90 C. Geochim Cosmochim Acta 54:1009–1017

Weissberg BG, Browne PRL, Seward TM (1979) Ore metals in active geothermal systems. In: Barnes HL (ed) Geochemistry of hydrothermal ore deposits. Wiley, New York, pp 738–780

White DE (1981) Active geothermal systems and hydrothermal ore deposits. Econ Geol 75th Anniv Vol:392–405

White G (1986) Puhipuhi mercury deposit. (Monograph Ser) Min Dep 26:193–198